Radiology

Functional and Targeted Lymph Node Imaging in Prostate Cancer: Current Status and Future Challenges[1]

Harriet C. Thoeny, MD
Sebastiano Barbieri, PhD
Johannes M. Froehlich, PhD
Baris Turkbey, MD
Peter L. Choyke, MD

Patients with prostate cancer who have regional lymph node (LN) metastases face an increased risk of death from disease and are therefore treated aggressively. Surgical LN dissection is the established method of staging regional nodes; however, this invasive technique carries substantial morbidities and a noninvasive imaging method is needed to reduce or eliminate the need for extended pelvic LN dissections (ePLND). Conventional computed tomography and magnetic resonance (MR) imaging have proven insensitive and nonspecific because both use nodal size criteria, which is notoriously inaccurate. Novel imaging techniques such as functional MR imaging by using diffusion-weighted MR imaging, MR lymphography with iron oxide particles, and targeted positron emission tomography imaging are currently under development and appear to improve LN staging of prostate cancer. Although progress is being made in staging nodes with imaging, it has not reached the point of replacing ePLND. In this review, the strengths and limitations of these new functional and targeted LN imaging techniques for prostate cancer are discussed.

[1] From the Department of Diagnostic, Pediatric, and Interventional Radiology, Inselspital University Hospital, Bern, Switzerland (H.C.T., S.B., J.M.F.); and Molecular Imaging Program, National Cancer Institute, National Institutes of Health, 10 Center Dr, Room B3B69F, Bethesda, MD 20892 (B.T., P.L.C.). Received August 13, 2016; revision requested September 27; revision received January 31, 2017; accepted February 24; final version accepted March 13. **Address correspondence to** P.C. (e-mail: *pchoyke@nih.gov*).

In patients with prostate cancer (PCa), the presence of lymph node (LN) metastases is a negative prognostic factor influencing treatment decisions and long-term survival (1). Currently, pelvic LN staging is primarily performed with computed tomography (CT) or magnetic resonance (MR) imaging by using size and shape criteria to define malignant nodes. However, these morphologic features are neither sensitive nor specific for LN metastases. For instance, micrometastases can be depicted in as many as 30% of normal-sized pelvic LNs (2,3), whereas LNs are often enlarged because of hyperplasia as a result of inflammatory or infectious diseases. Although morphologic imaging is limited, certain features such as loss of fatty hilum, irregular or ill-defined nodal margins beyond nodal size criteria, round shape in all three dimensions, lower signal intensity on T2-weighted images, and heterogeneous parenchymal signal can help to depict metastatic involvement in PCa nodal staging (4). However, such an approach is experience dependent and can be difficult to reproduce.

To frame the magnitude of the problem, the rate of LN-positive metastases with negative conventional imaging results varies 0%–26%, depending on clinical risk factors. For instance, for low-grade tumors the rate never exceeds 5%, whereas for high-grade tumors it can be much higher. Relapse rates up to 40% can be seen in patients who are node positive. Many of these patients may progress to eventual death. Therefore, accurate node staging is important (5).

The absence of a reliable imaging tool for nodal staging means that nodal staging depends mostly on the results of surgical node sampling. However, a long-standing debate exists as to whether an extended pelvic LN dissection (ePLND) or limited pelvic LN dissection (lPLND) should be performed in a particular patient. This decision often hinges on the risk status of the patient, which is based on clinical factors such as serum prostate-specific antigen, Gleason score, and imaging findings. Advocates of ePLND in patients with PCa point to evidence that it increases 5- and 10-year survival rates compared with lPLND when similar tumor stages are compared, but this evidence is still controversial (6). In that study, LN metastases were detected in 94 men (22.3% vs 77.7% for lPLND vs ePLND). Between these two groups, no difference was seen in the number of positive LNs (1.4 vs 1.8 for lPLND vs ePLND; P = .223) (3). In this series, at a median follow-up of 10.5 years, patients who underwent an ePLND had superior oncologic outcomes compared with those of the lPLND group, as follows: 5-year biochemical recurrence–free survival of 30.1% versus 7.1% (P = .018), 10-year metastasis-free survival of 62.2% versus 22.2% (P = .035), and 10-year cancer-specific survival of 83.6% versus 52.6% (P = .199). This analysis demonstrated an augmented improvement in biochemical recurrence–free survival in men with less than 15% positive nodes (6). In another prospective study, 406 patients with intermediate- or high-risk PCa according to the D'Amico criteria underwent either bilateral lPLND (n = 204) or ePLND (n = 202) and robot-assisted laparoscopic radical prostatectomy. Authors compared the perioperative course of patients undergoing robot-assisted lPLND or ePLND for PCa and examined the differential LN counts and rates of detection of LN metastases. They reported that the median operating time was 3.0 hours for the ePLND cohort and 2.8 hours for the lPLND cohort ($P < .001$). Mean intraoperative blood loss was 200 mL in both cohorts. Hospital stay was longer for a small percentage of patients in the ePLND cohort, with 75% of the ePLND cohort and 85% of the lPLND cohort staying 1 day (P = .004). No significant difference was found in the overall or major complication rates between the lPLND cohort (21.6% overall; 6.9% major) and ePLND cohort (22.8% overall; 4.5% major). Moreover, no difference was seen in the symptomatic lymphocele rate between the lPLND and ePLND groups (2.9% vs 2.5%, respectively). Overall, the LN-positive rate was 12% compared with 4% for the ePLND and lPLND groups, respectively (P = .002) (7). Although ePLND increases the detection of micrometastases that would otherwise go undetected, recent publications have shown that simply performing more complete histopathologic analysis of the nodes that are resected, whether by using ePLND or lPLND, may also increase the detection of nodal metastases. For instance, use of immunohistochemistry in addition to

Essentials

- Ultrasmall superparamagnetic iron oxide (USPIO)–enhanced MR imaging is capable of demonstrating small nodes involved by metastatic disease that fail to take up USPIO.
- Diffusion-weighted MR imaging is a promising method of depicting malignant nodes without any injection; however, the process is currently time consuming because nodes must be distinguished from small vessels.
- PET represents a promising new direction for lymph node imaging in prostate cancer because several new PET agents are highly sensitive and specific for prostate cancer, exemplified by prostate-specific membrane antigen–targeted agents.

https://doi.org/10.1148/radiol.2017161517

Content codes: GU MR

Radiology 2017; 285:728–743

Abbreviations:
ADC = apparent diffusion coefficient
CI = confidence interval
DCFBC = N-[N-[(S)-1,3-dicarboxypropyl] carbamoyl]-4-18F-fluorobenzyl-L-cysteine
DCFPyl = 2-(3-(1-carboxy-5-[(6-[18F]fluoro-pyridine-3-carbonyl)-amino]-pentyl)-ureido)-pentanedioic acid
DW = diffusion weighted
ePLND = extended pelvic lymph node dissection
FACBC = fluorocyclobutane-1-carboxylic acid
FDG = fluorodeoxyglucose
lPLND = limited pelvic lymph node dissection
LN = lymph node
PCa = prostate cancer
PSMA = prostate-specific membrane antigen
USPIO = ultrasmall superparamagnetic iron oxide

Conflicts of interest are listed at the end of this article.

standard histologic analysis increases detection rates of micrometastases by 28% (8). A more recent study included 54 patients with 1064 excised LNs in which 11 patients had evident metastases at standard pathologic examination, whereas seven patients had additionally detected occult metastases after serial section, immunohistochemistry, and real-time reverse transcriptase polymerase chain reaction evaluation. Use of serial section, immunohistochemistry, and reverse transcriptase polymerase chain reaction evaluation detected a higher percentage of patients with positive nodal metastases from 16.6% to 33.3%. Interestingly, the mean diameter of the 10 additional LNs with additionally detected occult metastases found at serial sections only and of the six additional LNs found at immunohistochemistry only was significantly lower than the mean diameter of the 28 metastases found at standard pathologic examination ($P < .0001$). Finally, patients with occult metastases showed a higher risk of biochemical recurrence compared with patients with no LN metastases ($P = .008$), indicating microscopic disease may have equal biologic significance to macroscopic disease (9). However, the long-term clinical impact of detecting such micrometastases by nonstandard pathologic techniques such as immunohistochemistry and reverse transcriptase polymerase chain reaction evaluation, as opposed to macrometastases visible at conventional staging, is yet to be determined.

Preoperative knowledge of the presence and precise location of suspicious nodes could greatly influence treatment. Ideally, a negative imaging test result would imply that surgery or radiation therapy could be confined to the prostate and node dissections would be unnecessary, whereas a positive imaging test result would necessitate the addition of other treatments such as extended radiation therapy with or without androgen deprivation therapy or pelvic LN dissection. Moreover, to be truly useful, the test would have to demonstrate few false-negative and false-positive LNs. In a series with 1740 patients who underwent radical prostatectomy and ePLND, 108 patients (6%) with positive LNs were identified. The median number of LNs removed was 17 (interquartile range, 11–24), and median follow-up was 26 months (interquartile range, 14–43 months). Ninety-one (84%) patients did not receive adjuvant androgen deprivation therapy, of whom 60% had biochemical recurrence with a median time to recurrence of 8 months. The 1- and 3-year biochemical recurrence–free probability was 42 and 28%, respectively. Patients with two or fewer positive LNs had significantly better estimated biochemical recurrence–free probability compared with those with more than two positive LNs ($P = .002$). The total number of positive LNs (hazard ratio, 1.1; 95% confidence interval [CI]: 1.01, 1.2; $P = .04$) and Gleason score 8–10 (hazard ratio, 1.96; 95% CI: 1.1, 3.4; $P = .02$) were predictors of biochemical recurrence at multivariate analysis. This study concluded that among men with positive LNs at time of robotic prostatectomy, those with two or fewer positive nodes and a Gleason score of less than 8 exhibited favorable biochemical recurrence–free survival without adjuvant therapy (10). This conclusion can imply that reliable preoperative information on nodal metastases burden can be helpful to tailor the treatment. Unfortunately, this ideal imaging technology does not currently exist. However, in recent years several new methods have been introduced that improve pelvic LN imaging by using functional MR imaging and targeted positron emission tomography (PET)/CT compared with conventional imaging. Promising results suggest that a variety of methods might be poised to take on the task of LN staging in PCa, including ultrasmall superparamagnetic iron oxide (USPIO)–enhanced MR imaging, diffusion-weighted (DW) MR imaging, a combination of these two methods, and PET/CT imaging with novel tracers (Table). Which of these methods is likely to become a reality? Along with this important question, it is critical to note that an ideal imaging method should be both sensitive and specific. However, a tradeoff always exists between these two parameters. If the imaging method is not sensitive enough, then clinicians will not rely on it except for high-risk cases. If the imaging method is nonspecific, (ie, has a high false-positive rate), then it could either be used to deny some patients curative therapy or result in more-aggressive-than-needed therapy, both undesirable outcomes. Thus, it is important that any LN staging test be both sensitive and specific. Although it is tempting to comment on the features of an ideal imaging modality for nodal staging, one should also comment on the ideal trial design in which the modality needs to be tested. Such a trial should include prospective randomization of patients to "with" or "without" imaging arms for evaluation of progression-free survival, time to metastases, and overall survival end points. Unfortunately, none of the imaging modalities we discuss in this article have been studied in that ideal design. The aim of this article is to summarize the current state of data supporting functional and targeted imaging methods in LN staging of patients with PCa.

USPIO-enhanced Imaging

USPIO-enhanced MR imaging has been widely studied for nodal staging of various malignancies, including PCa. Ferumoxtran-10 (no longer manufactured; was commercially known as Sinerem in Europe or Combidex in the United States, and was formerly produced by Advanced Magnetics, Cambridge, Mass) was the USPIO initially used in these studies. Ferumoxtran-10 is a dextran-coated USPIO that is injected intravenously at a dose of 2.6 mg of iron per kilogram over 30 minutes. More rapid infusion rates have been associated with adverse events such as back pain, hypersensitivity reactions (merging pruritus, urticaria, rash, and erythema), hypotension, and chest pain (11). After it is injected, the agent leaks into the extravascular space but is taken up via lymphatics into nodes where it is engulfed by macrophages within 24–36 hours after administration. Where normal macrophages are abundant (ie, in

Sensitivity, Specificity, PPV, and NPV of Currently Available Functional and Targeted Imaging Methods for LN Staging of PCa

Variable	Authors	Disease Phase	No. of Patients	Validation Method	Sensitivity (%)	Specificity (%)	PPV (%)	NPV (%)
USPIO (ferurmoxtran-10)	Harisinghani et al (14)	Localized	80	Histopathologic analysis (surgery)	100	95.7	94.2	100
USPIO (ferumoxtran-10)	Heesakkers et al (15)	Localized	296	Histopathologic analysis (biopsy or surgery)	…	…	76	…
USPIO (ferumoxtran-10)	Heesakkers et al (17)	Localized	375	Histopathologic analysis (surgery)	82	97	69	96
USPIO (ferumoxytol)	Harisinghani et al (25)	Localized	10	Histopathologic analysis (surgery)	…	…	…	…
DW MR imaging	Thoeny et al (4)	Localized	120	Histopathologic analysis (surgery)	72.7	86.2	…	…
USPIO (ferumoxtran-10) + DW MR imaging	Thoeny et al (37)	Localized	21	Histopathologic analysis (surgery)	60–80	80–93	50–80	86–93
USPIO (ferumoxtran-10) + DW MR imaging	Birkhauser et al (36)	Localized	75	Histopathologic analysis (surgery)	65–75	93–96	…	…
^{18}F-FDG PET	Beauregard et al (38)	Localized	54	Histopathologic analysis (surgery) + clinical follow-up	27	…	…	…
^{11}C-choline PET	Vag et al (39)	Localized	33	Histopathologic analysis (surgery)	69.72	90.48	…	…
^{11}C-chofine PET	Fanti et al (40)	BCR	752 (meta-analysis)	Histopathologic analysis (surgery or biopsy) + clinical follow-up	36	…	…	…
^{18}F-choline PET	Poulsen et al (42)	Localized	210	Histopathologic analysis (surgery)	73.2	87.6	58.8	93.1
^{18}F-choline PET	Evangelista et al (43)	Localized	441(meta-analysis)	Histopathologic analysis (surgery)	49.2	95	…	…
^{11}C-acetate PET	Schumacher et al (45)	Localized	19	Histopathologic analysis (surgery)	90	67	75	86
^{11}C-acetate PET	Mohsen et al (47)	Localized, BCR	…	…	73	79	…	…
^{18}F-DCFBC PET	Rowe et al (57)	Metastatic	19	Clinical follow-up	92	NA	…	…
^{68}Ga-PSMA PET	Budaus et al (63)	Localized	30	Histopathologic analysis (surgery)	33.3	100	100	52.9
^{68}Ga-PSMA PET	Afshar-Oromieh et al (61)	BCR	42	Histopathologic analysis (but details not specified)	76.6	100	91.4	100
^{68}Ga-PSMA PET	Hijazi et al (64)	Localized	35	Histopathologic analysis (surgery)	94	99	89	99.5
^{68}Ga-PSMA PET	Rauscher et al (65)	BCR	48	Histopathologic analysis (surgery)	77.9	97.3	…	…

Note.—PPV = positive predictive value, NPV = negative predictive value, BCR = biochemical recurrence, ^{18}F = fluorine 18, FDG = fluorodeoxyglucose, ^{11}C = carbon 11, DCFBC = N-[N-[(S)-1,3-dicarboxypropyl]carbamoyl]-4-18F-fluorobenzyl-L-cysteine, ^{68}Ga = gallium 68, PSMA = prostate-specific membrane antigen.

normal LNs), the accumulation of intracellular iron oxide causes T2 shortening, leading to a signal decrease on T2 and T2*-weighted images. However, regions of the LN replaced by metastases, having few macrophages, will not take up the USPIO and, thus, remain unchanged in signal intensity compared with baseline (Figs 1–4). Therefore, nodes completely replaced with metastases will not take up the USPIO and be both uniform and unchanged in signal, whereas partially replaced metastatic nodes will become heterogeneous in signal intensity. USPIO-enhanced imaging typically requires two imaging sessions, a baseline image prior to injection and an image obtained 24–36 hours after contrast medium administration. However, one study has suggested that only images obtained after USPIO enhancement can be sufficient for image interpretation, allowing the baseline image to be skipped; moreover, interpretation of such images can require considerable experience (12). Some malignant LNs are already hypointense on T2 and T2*-weighted images (13), and this method may not be applicable in those cases. A prospective study of ferumoxtran-10–enhanced MR imaging was performed in 80 patients with PCa (14). In this study, 334 LNs were

Figure 1

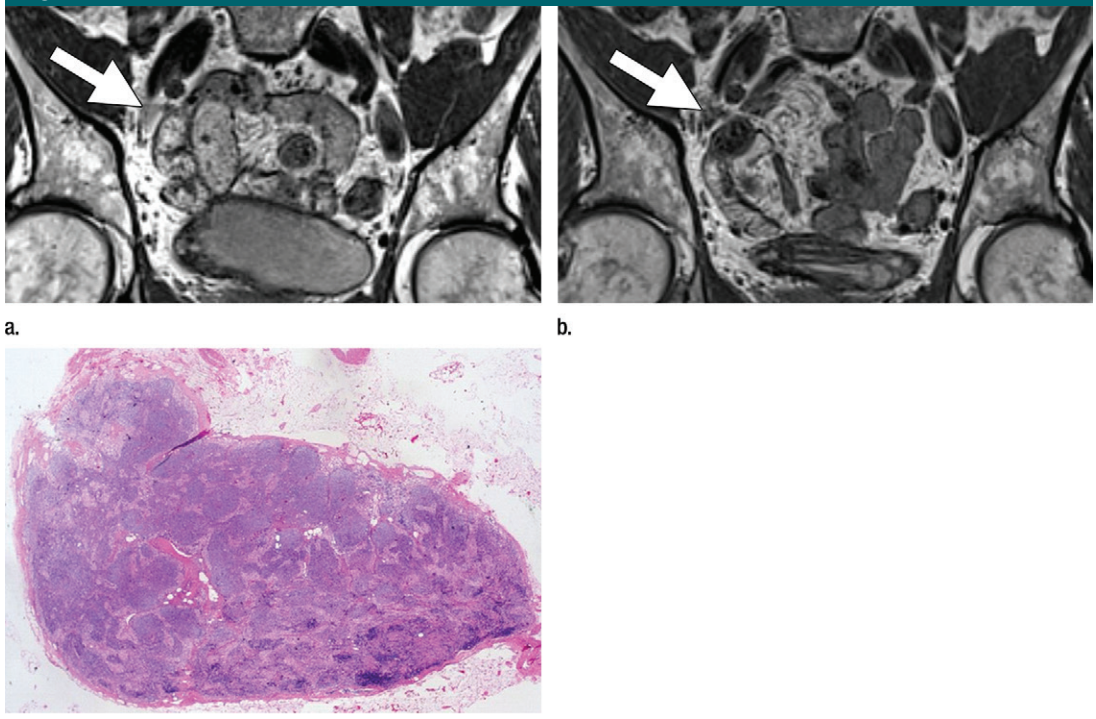

a. b. c.

Figure 1: Images in a 69-year-old man with PCa (stage pT2pN0, Gleason score 3+4 = 7). **(a)** Coronal three-dimensional T2-weighted MR image (repetition time msec/echo time msec, 640/47) shows longitudinal LN (11 mm × 8 mm) in external iliac region on the right (arrow). **(b)** MR image 36 hours after intravenous administration of ferumoxtran-10 with identical parameters as in **a** shows partial uptake suspicious of a metastatic LN. **(c)** Photomicrograph (hematoxylin-eosin stain) demonstrates follicular hyperplasia and no signs of metastatic involvement.

Figure 2

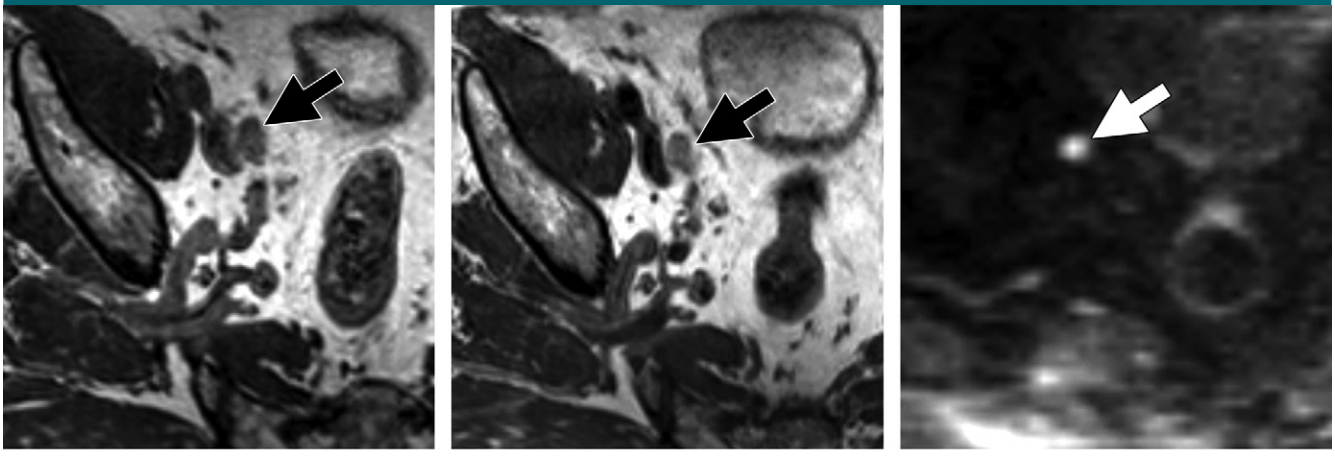

a. b. c.

Figure 2: Images in a 64-year man with PCa (stage pT3bpN1, Gleason score 4+4 = 8). **(a)** Reconstructed axial T2-weighted MR image (640/47) shows LN in external iliac region on the right (arrow) before and **(b)** 36 hours after intravenous administration of ferumoxtran-10 with lack of contrast medium uptake (no signal change) suspicious for a LN metastasis. **(c)** Axial DW (*b* value, 1000 sec/mm^2) MR image after ferumoxtran-10 administration shows hyperintense round structure (arrow) corresponding to LN metastasis at histologic examination.

Figure 3

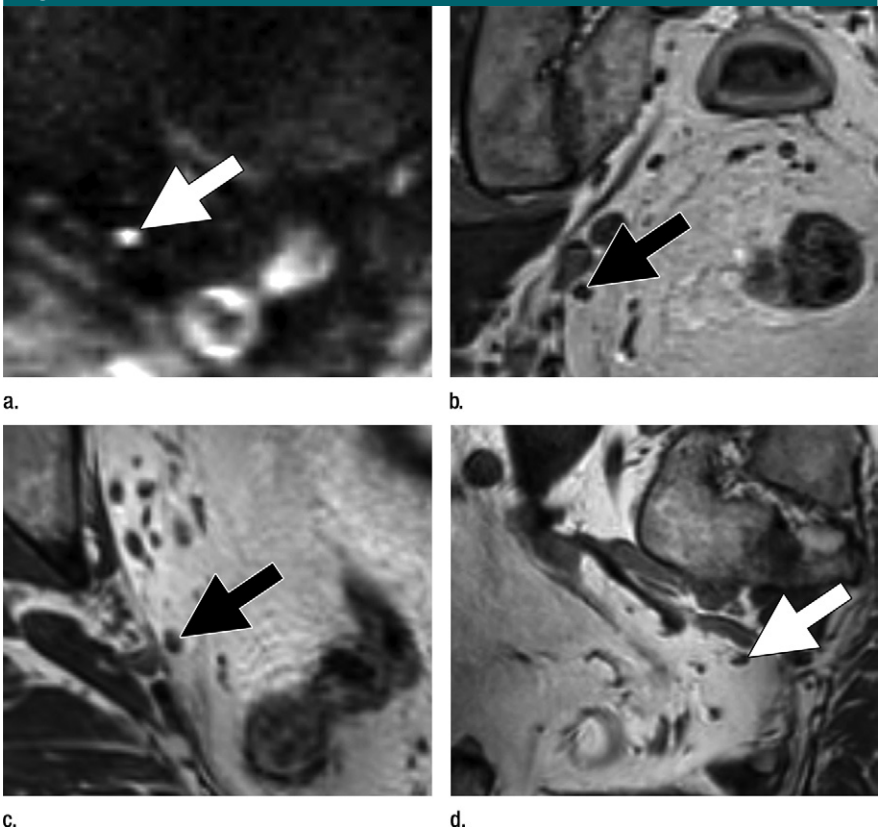

Figure 3: Images in a 63-year man with PCa (stage pT4apN1, Gleason score 4+5 = 9). **(a)** Axial DW (*b* value, 1000 sec/mm^2) MR image shows hyperintense, round, noncontinuous structure (arrow) corresponding to round irregular LN in external iliac region on the right on **(b)** coronal three-dimensional T2-weighted image (sampling perfection with application optimized contrasts using different flip-angle evolution, 640/47) as well as on **(c)** axial reconstructed and **(d)** sagittal reconstructed three-dimensional T2-weighted images suspicious for LN metastasis, confirmed at histologic examination.

resected (only lPLND was performed) or biopsied for validation. At histopathologic analysis, metastases were detected in 63 nodes (19% of resected nodes) from 33 patients (41%). Among these 63 nodes, 45 (71%) did not fulfill the usual size criteria for malignancy at CT yet were nonetheless suspicious at ferumoxtran-10–enhanced MR imaging. In this study, 100% of patients with surgical nodal metastases were identified, and a node-by-node analysis had a significantly higher sensitivity than did conventional MR imaging (90.5% vs 35.4%; $P < .001$) or nomograms (14). However, the negative predictive value of ferumoxtran-10 in this study has to be interpreted with caution because these patients did not undergo ePLND; therefore, the negative predictive value may be underestimated.

USPIO-enhanced MR imaging has also been used in staging several tumor types including bladder, rectal, and gynecologic cancers as well as PCa. Excellent results have been reported, with diagnostic accuracies up to 97.3% (14–18). Most of these studies included patients with nodes of varying size including enlarged nodes, and results were validated with either biopsy or lPLND again resulting in an understaging bias (19). A recent prospective study including 75 patients with bladder cancer and/or PCa and normal-sized LNs at preoperative cross-sectional imaging used ePLND as the reference standard. A total of 2993 normal-sized nodes were resected and analyzed by using histopathologic analysis. Among three readers, the average sensitivity of USPIO-enhanced MR imaging was 50%, with a specificity of 88.4% and a diagnostic accuracy of 81.8% (20). Although the sensitivity of the method is somewhat disappointing in absolute terms, relative to other methods of depicting metastases in normal-sized nodes, these results represent an advance.

However, several significant challenges exist to USPIO-enhanced MR imaging. The first is the availability of the agent. Ferumoxtran-10 is currently only available in the Netherlands, where it is made privately. The drug itself has been discontinued by the commercial manufacturer, and thus there is extremely limited access to it. The method is also logistically inconvenient, requiring both a baseline image and an image after injection, which must be obtained on consecutive days and requires several visits to the imaging center by the patient. Image interpretation is highly subjective and laborious because every node must be compared on both sequences before and after injection. Metastases smaller than 5 mm in diameter can be missed because of spatial resolution limits. Enlarged but benign nodes can fail to take up USPIO because of severe inflammation or fibrosis, leading to false-positive results. Furthermore, ferumoxtran-10 must be administered slowly through a filtered needle to minimize infusion reactions including hypersensitivity and back pain (21).

Ferumoxytol, a USPIO that is similar to ferumoxtran-10 in concept, addresses some of these limitations. First, ferumoxytol has been approved by the U.S. Food and Drug Administration as an iron replacement therapy for patients with anemia related to chronic kidney failure, and thus is more available (22,23) than is ferumoxtran-10. Ferumoxytol is a semisynthetic carbohydrate-coated magnetic iron oxide preparation that can be administered as a bolus (24). However, a significant disadvantage of ferumoxytol is that it requires substantially higher doses of iron to achieve similar results to ferumoxtran-10.

Figure 4

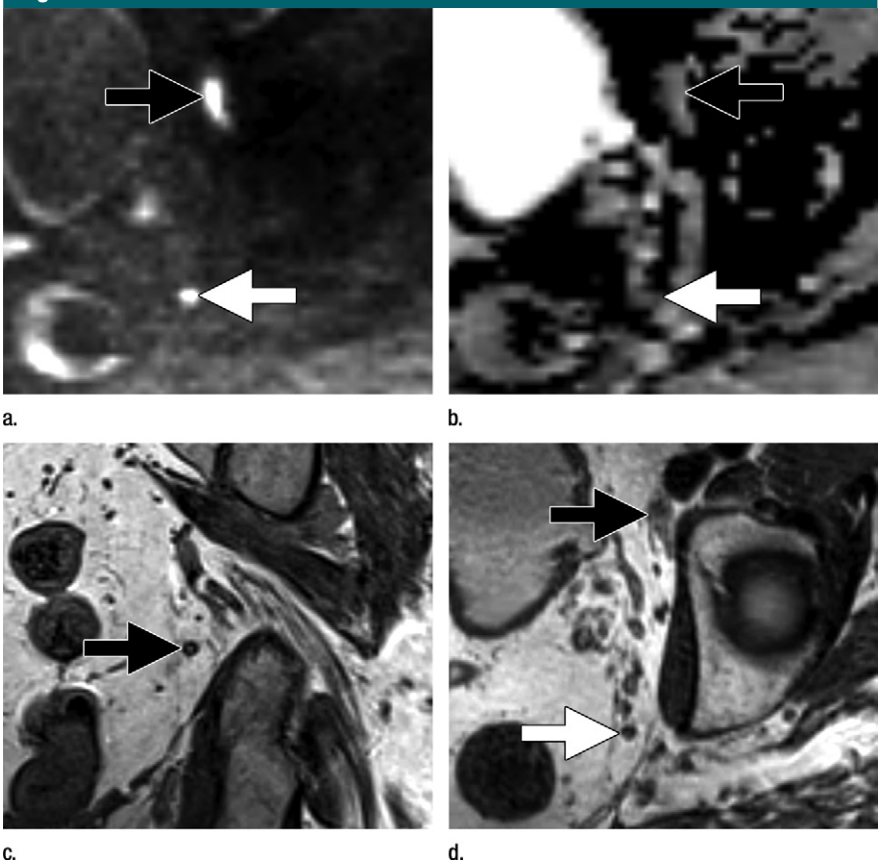

Figure 4: Images in a 65-year man with PCa (stage pT3bpN1, Gleason score 3+4 = 7). **(a)** Axial DW (*b* value, 1000 sec/mm^2) MR image shows hyperintense, round, noncontinuous structure (white arrow) corresponding to hypointense structure on **(b)** corresponding apparent diffusion coefficient (ADC) map (ADC, 826 × 10−6 mm^2/sec). **(c)** Coronal three-dimensional T2-weighted image (sampling perfection with application optimized contrasts using different flip-angle evolution, 640/47) confirms presence of round hypointense LN in internal iliac region on the left as well as on **(d)** axial three-dimensional T2-weighted image corresponding to LN metastasis. A second large LN (black arrow) shows presence of fat, is elongated and also presents hyperintense pattern on the DW image (**a**). However, average ADC of this LN is 1082 × 10−6 mm^2/sec and it is not metastatic.

Whereas adequate darkening of the normal LNs was achieved at a dose of only 2.6 mg Fe/kg with ferumoxtran-10, doses of 4–7.5 mg Fe/kg are needed to achieve similar results with ferumoxytol. Initial reports suggested a dose of 4 mg Fe/kg would be needed for MR lymphography based on a 10-patient study. MR imaging was performed before and at 5 hours, 18 hours, and 24 hours following ferumoxytol injection. Among the 26 LNs with histopathologic confirmation, ferumoxtyol helped to correctly identify all 20 benign and six malignant nodes. Ferumoxytol caused a significant decrease in signal intensity within benign nodes, but little change in signal within malignant nodes. Moreover, the reported maximum contrast was obtained 24 hours after injection (25). However, this study is limited by its small size. Recently, a pilot study of 15 patients revealed that the percentage of signal decrease in LN signal at 24 hours after ferumoxytol injection for all normal LNs was −36.4%, −45.4%, and −65.1% for doses of 4 mg Fe/kg, 6 mg Fe/kg, and 7.5 mg Fe/kg, respectively (P = .041). At doses of 4 mg Fe/kg and 6mg Fe/kg, heterogeneous loss of signal was observed in normal nodes. Therefore, this study indicated that a dose of 7.5 mg Fe/kg is required to accurately use ferumoxytol for LN mapping to reduce false-positive readings (26) (Fig 5). This dose is slightly higher than the recommended dose of approximately 6 mg Fe/kg approved by the Food and Drug Administration for indication of iron replacement therapy for most patients. No large studies have proven that ferumoxytol produces results comparable to ferumoxtran-10, and future studies are needed to better validate the utility and practicality of ferumoxytol-enhanced MR lymphography. Finally, it should be noted that nodal imaging with ferumoxytol is considered off-label use and is not recommended for general use. The Food and Drug Administration has also announced a drug safety communication for ferumoxytol with strengthened warnings and revised prescribing instructions, which included recommendations such as only administration of intravenous iron products to patients who require intravenous iron therapy, avoidance of administration of ferumoxytol to patients with a history of allergic reaction to ferumoxytol or other intravenous iron products, and administration of diluted ferumoxytol as an intravenous infusion over a minimum of 15 minutes but not as an undiluted intravenous injection. Additionally, the Food and Drug Administration recommended the close monitoring of patients for signs and symptoms of serious allergic reactions, including monitoring blood pressure and pulse during ferumoxytol administration and for at least 30 minutes following each infusion; careful consideration of the potential risks and benefits of ferumoxytol administration in older patients with multiple or serious medical conditions, because these patients may experience more severe reactions; and consideration of the potential risks and benefits of ferumoxytol administration in patients with a history of multiple drug allergies (27).

Figure 5

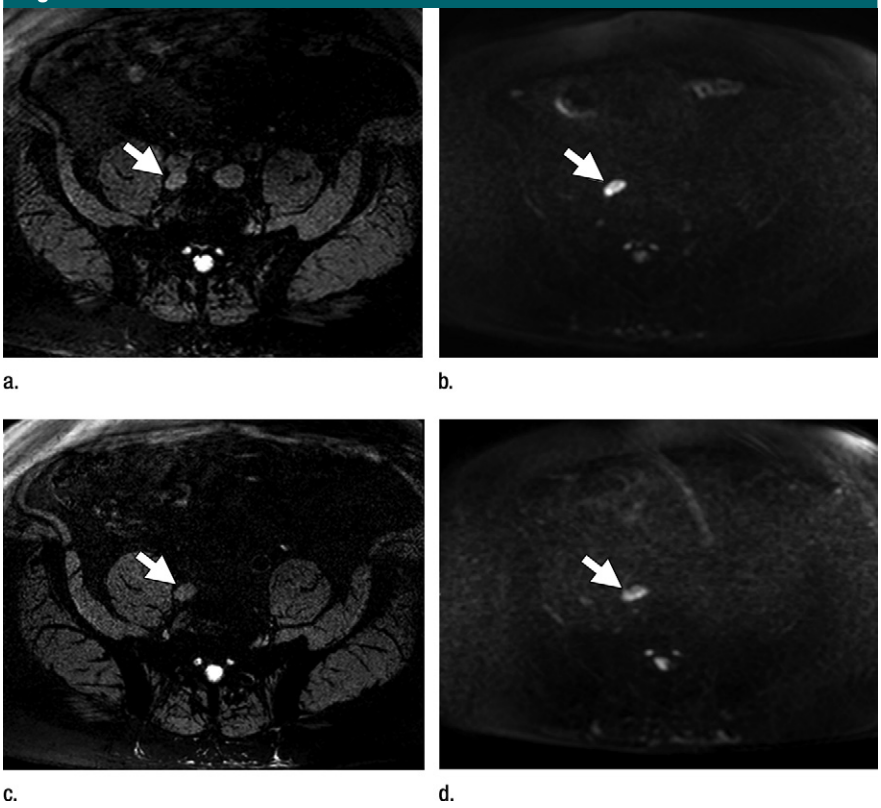

Figure 5: Images in a 67-year-old man after external beam radiation therapy for Gleason 4+5 PCa with a current prostate-specific antigen of 2.01 ng/mL. **(a)** Axial T2*-weighted MR image prior to ferumoxytol injection shows hyperintense LN in right common iliac chain (arrow). **(b)** LN shows hyperintense signal pattern on DW MR image (*b* value, 800 sec/mm^2) (arrow). **(c)** Axial T2*-weighted MR image at 24 hours after injection of 7.5 mg Fe/kg ferumoxytol and **(d)** DW MR image (*b* value, 800 sec/mm^2) show maintenance of hyperintense signal pattern, indicating lack of ferumoxytol uptake within this LN (arrow in **c** and **d**). Findings are consistent with PCa metastases within this right common iliac chain LN.

DW MR Imaging

DW MR imaging is a noninvasive MR imaging technique that reflects how the underlying structure of the tissue limits the random Brownian motion of water molecules within the tumor. It has been shown that most tumors exhibit impeded diffusion because of changes in the volume of epithelium, stroma, and lumen space (28,29). Therefore, it is predicted that LNs harboring malignancy will have impeded diffusion to the extent the node is replaced with tumor.

Nodes can be identified on high-*b*-value images (preferably *b* value of 1000 sec/mm^2) as round discrete structures. There should be careful correlation of the DW MR images with morphologic images (preferably T2-weighted images obtained in three dimensions) for correct image interpretation because, for instance, the presence of a fatty hilum can rule out a malignant node. DW MR imaging has been used for pelvic LN staging of bladder cancer and PCa, as well as for various gynecologic malignancies. Previous studies have used the ADC as a parameter to differentiate benign from malignant nodes, with lower ADC values suggesting metastatic nodes. However, the threshold ADC value has varied among studies, suggesting that it may currently be impossible to establish a universal ADC threshold value across different MR imaging vendors, institutional implementations, and methods of calculation. Differing variety of *b* values and mean, median, and minimum ADC values or ADC values relative to the renal cortex as indexes of malignancy have been used, suggesting that a need exists for standardization (30–32). Overall, studies that use ADC maps to help detect pelvic LN metastases have reported sensitivities ranging 76.4%–100% and specificities ranging 74%–98.3% (33). Studies also show no significant difference in ADC between benign and malignant nodes (4,34). Although malignant LNs seem to have lower ADC values compared with benign LNs, the overlap is substantial; therefore, ADC measurement alone is not recommended for diagnosing nodal metastases. Regardless of the method used, DW MR imaging is also prone to susceptibility artifacts caused by air within the bowel and to motion artifacts. Therefore, antiperistaltic drugs can be administered, if available, to decrease motion artifacts because of bowel peristalsis.

An alternative to ADC mapping is to use high-*b*-value images. This method is highly sensitive for detecting voxels with the most limited diffusion, because such voxels retain signal while voxels containing normal tissue rapidly decrease in signal, thereby creating high-contrast images. Because diffusion in metastatic LNs is impeded, the signal intensity of metastatic nodes obtained at high *b* values will be increased compared with that of surrounding normal tissue. Thus, high-*b*-value images (usually acquired at a *b* value of 1000 sec/mm^2 or higher) will reveal positive nodes as hyperintense, round, and noncontinuous structures that correlate with morphologic T2 images. A limitation of this method is that the signal-to-noise ratio of high-*b*-value DW MR imaging is much lower than that of conventional images, decreasing sensitivity. Nevertheless, by using 3.0-T MR imaging with optimized surface coils, a recent study used high-*b*-value imaging in patients with bladder cancer or PCa undergoing ePLND. In this study, meticulous morphologic analysis of normal-sized nodes on three-dimensional T2-weighted and DW MR images

was performed, resulting in sensitivities ranging from 75.8% (95% CI: 60.7, 89.3) to 81.8% (95% CI: 67.6, 93.9) and specificity of 95.4% (95% CI: 90.4, 98.9) for both readers, with diagnostic accuracies between 90% (95% CI: 83.3, 94.2) and 91.7% (95% CI: 85.8, 95.8) on a per-patient level (30). In another study with 27 patients, T2-weighted MR imaging was compared with fused T2-weighted MR imaging and DW MR imaging for depiction of metastatic LNs. Fused T2-weighted MR imaging and DW MR imaging depicted more LNs (161 vs 114) and the detected LNs on fused images were smaller compared with ones depicted at T2-weighted MR imaging alone (3.7 mm vs 4.7 mm; $P = .007$) (35). Thus, high-*b*-value DW MR imaging is a highly promising, minimally invasive method of depicting malignant nodes. Its great advantage is that it is potentially widely available, is nonquantitative, and does not require injection of an exogenous agent (Figs 2–4). However, high-*b*-value DW MR imaging requires great care when interpreting because the nodes are often quite small, the images are noisy, and careful correlation with morphologic images is needed to avoid mistaking vessels, nerves, or other structures for nodes. A positive DW MR imaging result can provide a roadmap for the surgery or radiation therapy plan if suspicious nodes are seen outside the surgical template or radiation field. However, because the false-negative rate of DW MR imaging can be too high, a negative pelvic DW MR imaging result cannot be used to rule out the need for ePLND if otherwise indicated.

Combining USPIO-enhanced MR Imaging and DW MR Imaging

A combination of USPIO enhancement and DW MR imaging might further improve depiction of LN metastases. USPIO uptake in normal LNs leads to signal loss both on T2-weighted and on high-*b*-value DW MR images because the iron markedly reduces T2. Therefore, benign LNs are not visible on high-*b*-value images, whereas malignant LNs remain hyperintense on the high-*b*-value images because of lack of contrast medium uptake (36,37).

As before, USPIO has to be administered 24–36 hours prior to imaging, but only the image after injection is needed. Imaging should include a three-dimensional T2-weighted sequence in addition to a DW MR imaging sequence covering the entire pelvis.

For image interpretation, the high-*b*-value images are assessed for the presence of round, discrete, and hyperintense structures and correlated with morphologic images. If these structures correspond to LNs, then they are assumed to be malignant, whereas benign LNs are invisible on the high-*b*-value images after USPIO enhancement.

This approach has the benefits of being faster to interpret and easier to perform. However, a USPIO still has to be administered, making the study more invasive and costly. Furthermore, even though the imaging is only performed once, the patient has to come to the hospital twice because USPIO has to be administered at least 24 hours prior to MR imaging.

There are only two studies applying the combination of USPIO enhancement and DW MR imaging in patients with bladder cancer and/or PCa by using pelvic LN dissection as the reference standard in a total of 75 patients. Only normal-sized LNs at preoperative cross-sectional imaging were included. The reported sensitivities of three readers ranged 65%–75% and specificities ranged 93%–96% on a per-patient basis (36,37). The sensitivities on a per–pelvic side basis ranged 58%–67% and the specificities ranged 94%–97%. Thus, the combination of USPIO enhancement and DW MR imaging had lower sensitivity than did DW MR imaging alone based on the current, albeit limited, literature.

Novel PET Tracers

The multiple advantages of MR imaging include its lack of ionizing radiation, high spatial resolution, and wide availability; however, there are also disadvantages. Abnormalities in DW MR imaging can be nonspecific. The promise of PET/CT is that it can be highly sensitive and specific. However, in addition to the disadvantage of ionizing radiation and cost, spatial resolution is markedly inferior to MR imaging. To some extent, this limitation can be compensated by the concomitant use of CT or MR imaging. However, both PET/CT and PET/MR imaging cannot overcome a fundamental limitation, which is partial volume averaging because of larger voxel dimensions of PET scans. This effectively reduces sensitivity for small lesions. This limitation can only be overcome if there is specific uptake by the PET agent in the lesion of interest.

The use of PET/CT imaging has increased because of the widespread availability of scanners and increased access to commercial radiopharmaceutical production facilities. ^{18}F-FDG, which targets the glycolytic pathway, is the most commonly used radiotracer in oncology; however, it has known limitations in PCa. As a result, a variety of other novel targeted PET radiotracers have been developed for LN staging in PCa. Below, we review available PET radiotracers that have been used in clinical trials for detecting nodal metastases in PCa.

FDG PET

FDG PET/CT, the most commonly available PET agent in oncology, has been disappointing in the staging of LNs in PCa. The main reasons for this are the relatively low glycolytic activity of PCa compared with that of other cancer types, activity in the ureter and bladder obscuring visualization, and overlap in uptake pattern of inflammation and metastases. Although some PCas do take up FDG, most do not and it has greatly lowered enthusiasm for its use in staging. This lowered enthusiasm is evident in the relatively small number of studies that have been published on the subject in recent years. In one of the few, a study of 41 patients undergoing FDG PET/CT prior to PCa surgery revealed a sensitivity of only 27% for LN metastases (38). Thus,

Figure 6

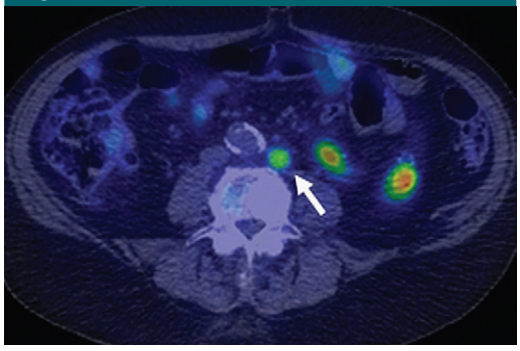

Figure 6: Image in an 82-year-old man after radical prostatectomy and LN dissection for Gleason 4+3 PCa 5 years ago with current prostate-specific antigen of 1.6 ng/mL. Axial ^{11}C-choline PET/CT image shows specific tracer uptake within left retroperitoneal LN (standardized uptake value, 6) (arrow). CT-guided biopsy of this node revealed metastatic prostate cancer involvement. (Image courtesy of Dr Adam T. Froemming, Mayo Clinic, Rochester, Minn.)

FDG PET/CT is not a viable method for LN staging in PCa.

Choline PET

Choline is incorporated into cell membranes as phosphatidylcholine and, therefore, uptake of radiolabeled choline reflects cell membrane production, such as occurs in cancers during proliferation. Because benign processes such as chronic inflammation can also cause cell membrane production, choline scans can be nonspecific. Choline can be radiolabeled with either ^{11}C or ^{18}F. ^{11}C has a half-life of only 20 minutes, and thus its use is limited to institutions with cyclotrons and radiochemistry facilities. One advantage of ^{11}C-choline is that it is not excreted immediately in the urinary tract, leaving the pelvic area free of urinary activity (Fig 6). In a prospective study of ^{11}C-choline, 33 patients underwent DW MR imaging and ^{11}C-choline PET/CT prior to prostatectomy and ePLND. A significant difference in mean standardized uptake value between benign and malignant LNs was observed (1.61 vs 3.20; $P < .001$); however, overlap was present between the two categories. The optimal threshold for mean standardized uptake value with ^{11}C-choline was 2.5, resulting in a sensitivity and specificity of 70% and 90%, respectively (39). A recent meta-analysis focusing on ^{11}C-choline PET/CT for nodal staging analyzed a total of 10 studies with histopathologic verification. The overall detection rate for ^{11}C-choline PET was 36% (median, 31%; range, 9%–84%) even though some of the studies included patients with biochemical recurrence, which would be expected to be more aggressive than would primary diagnosis (40). Thus, ^{11}C-choline demonstrates variable performance in staging LNs in PCa and feasibility issues with its production make it challenging for many medical centers to use.

^{18}F-choline or fluorocholine is an alternative method of performing PET imaging with choline. It has the advantage of a longer-lived PET emitter (110 minutes) but demonstrates more urinary excretion and higher background than does ^{11}C-choline. Fluorocholine can be synthesized as fluoromethylcholine or fluoroethylcholine, although it is unclear whether significant performance differences exist (41). A prospective study of ^{18}F-fluoromethylcholine PET/CT in 210 patients with PCa undergoing preoperative LN staging and subsequent LN dissection revealed metastatic LNs in 41 patients. The sensitivity, specificity, positive predictive value, and negative predictive value of ^{18}F-fluoromethylcholine PET/CT on a per-patient basis were 73.2%, 87.6%, 58.8%, and 93.1%, respectively. However, the corresponding values on a per-LN basis were 56.2%, 94%, 40.2%, and 96.8%, suggesting a low false-positive rate but a high false-negative rate (42). A meta-analysis of 10 studies evaluating ^{18}F-fluoromethylcholine PET/CT for nodal staging prior to definitive therapy revealed a pooled sensitivity and specificity of 49% and 95%, respectively. Results of these trials and metadata collectively suggest that ^{18}F-fluoromethylcholine PET/CT tends to have modest sensitivity but high specificity (43).

^{11}C-Acetate PET

Fatty acid synthase, for which acetate is a substrate, is reported to be overexpressed in PCa. Therefore, there is increased uptake of acetate in PCa (44). ^{11}C-acetate has been studied as a means to localize and stage PCa. In a study of 19 patients who underwent radical prostatectomy and ePLND, ^{11}C-acetate PET/CT demonstrated a per-patient sensitivity, specificity, and positive predictive value of 90%, 67%, and 75%, respectively. On a per–nodal region basis, sensitivity, specificity, positive predictive value, and negative predictive value were 62%, 89%, 62%, and 89%, respectively (45). Thus, this agent also shows a relatively low false-positive rate but only a modest sensitivity. Another prospective study investigating ^{11}C-acetate PET/CT for preoperative staging found a sensitivity, specificity, positive predictive value, and negative predictive value of 68.0%, 78.1%, 48.6%, and 88.9%, respectively (46). Another meta-analysis of ^{11}C-acetate in PCa reported a pooled sensitivity of 73% (range, 54%–88%) and a pooled specificity of 79% (range, 72%–86%) (47). However, it is difficult to compare studies because the severity of disease is not controlled in this meta-analysis (47). Thus, although the results of ^{11}C-acetate PET overlap those of ^{11}C-choline and ^{18}F choline PET, it is safe to conclude no advantage exists to

Figure 7

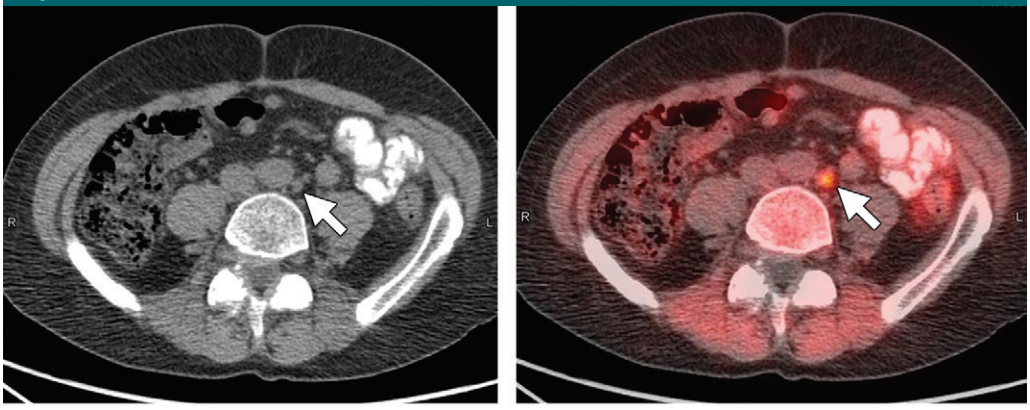

a. b.

Figure 7: Images in a 70-year-old man after radical prostatectomy and radiation therapy with current prostate-specific antigen of 8.9 ng/mL despite androgen deprivation therapy. **(a)** Axial CT image shows a subcentimeter LN in left retroperitoneum (arrow). **(b)** Axial ^{18}F-FACBC PET/CT image shows specific uptake within left retroperitoneal LN (standardized uptake value, 6) (arrow). (Image courtesy of Dr David Schuster, Emory University, Atlanta, Ga.)

^{11}C-acetate and there may be a slightly inferior performance. However, in reality it is difficult to compare these agents across different study populations with different severity of disease. Like ^{11}C-choline, ^{11}C-acetate has a short half-life and is impractical for most health care settings. Additionally, some studies report low sensitivity and specificity, indicating ^{11}C-acetate may not be the ideal radiotracer for nodal staging of PCa.

^{18}F-Fluorocyclobutane-1-Carboxylic Acid

Anti-^{18}F-fluorocyclobutane-1-carboxylic acid (FACBC) is a synthetic L-leucine analog that demonstrates uptake in PCa. Many tumors transport amino acids across the cell membranes at increased rates, presumably to meet the increased demands of protein synthesis. One such amino acid, leucine, appears to be taken up in PCa cells (48). There is less widespread experience with ^{18}F-FACBC than with choline and acetate compounds. In one small study validated with ePLND, seven of nine patients with positive nodes were positive at ^{18}F-FACBC imaging. Malignant LN uptake in both the staging and restaging patients was significantly higher than was benign nodal uptake (49). One head-to-head study of ^{18}F-FACBC PET/CT and ^{11}C-choline PET/CT involved 28 patients. On a per-patient basis, ^{11}C-choline PET/CT was positive in five patients and negative in 23 patients (detection rate, 17.8%), whereas ^{18}F-FACBC PET/CT was positive in 10 patients and negative in 18 (detection rate, 35.7%). All lesions that were positive with ^{11}C-choline were also positive at ^{18}F-FACBC PET/CT. ^{18}F-FACBC revealed nine LN metastases, whereas only two of these foci were revealed by using ^{11}C-choline PET/CT (50). This limited data suggest that ^{18}F-FACBC PET/CT is superior to ^{11}C-choline. However, the majority of nodal staging experience for ^{18}F-FACBC is in the setting of recurrent disease, and this tracer has recently been approved by the Food and Drug Administration for this indication (Fig 7).

PSMA Targeting PET Tracers

PSMA is a transmembrane protein that is highly expressed in PCa. Increased expression of PSMA is associated with higher grade, hormone-refractory, and metastatic disease (51). Accessible PSMA expression is normally low in normal prostate glandular epithelium and benign prostatic hyperplasia but increases in PCa cells; moreover, its expression is significantly upregulated in androgen-independent PCa. As such, PSMA is an excellent target for revealing PCa cells, and several molecular imaging approaches targeting PSMA are currently being investigated. The initial approach to PET imaging of PSMA was to use radiolabeled monoclonal antibodies directed against the intracellular domain of PSMA. Indium 111 (^{111}In)–capromab pendetide (ProstaScint; Aytu Bioscience, Englewood, Colo) was approved by the Food and Drug Administration in 1996 as a gamma camera and/or single-photon emission CT (SPECT) agent. However, because the target of capromab pendetide is intracellular, cell membranes must be disrupted to allow binding, which is an important limitation of this tracer. In addition to this limitation, nonspecific binding, high blood pool activity. and inferior spatial resolution of SPECT pose further hurdles to routine use. Thus, ^{111}In–capromab pendetide has significant limitations in evaluating nodal metastases (52). Subsequently, anti-PSMA antibodies have been developed that bind to the external domain of PSMA (53,54). None of these antibodies are currently commercially available but investigational studies have been promising.

Figure 8

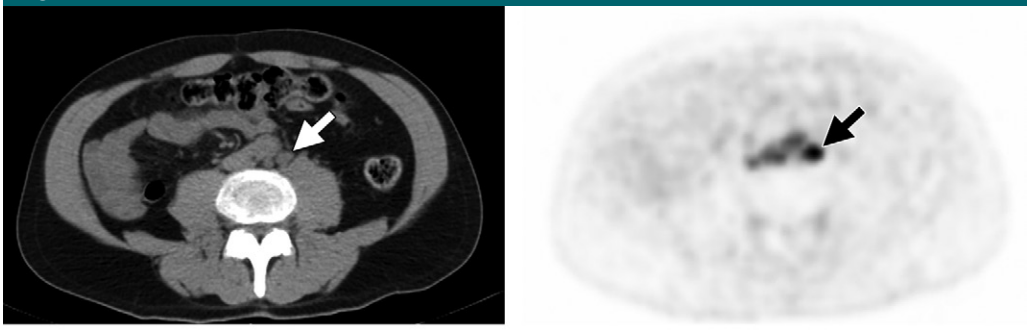

a. b.

Figure 8: Images in a 59-year-old man after radical prostatectomy and LN dissection for Gleason 4+3 PCa 8 years ago with current prostate-specific antigen of 11.57 ng/mL. **(a)** Axial CT image shows subcentimeter LN in left retroperitoneum (arrow). **(b)** Axial ^{18}F-DCFBC PET image shows specific uptake within left retroperitoneal LN (standardized uptake value, 8) (arrow).

More recently, a urea-based small molecule N-[N-[(*S*)-1,3-dicarboxypropyl]carbamoyl]-4-^{18}F-fluorobenzyl-L-cysteine (^{18}F-DCFBC) was shown to target the external domain of PSMA (55). Early clinical studies have shown promising results and others are currently underway (NCT02190279) to determine the efficacy of ^{18}F-DCFBC (56). ^{18}F-DCFBC was the first ^{18}F-labeled PSMA-targeting PET agent to be used clinically. In a prospective trial of 16 patients, ^{18}F-DCFBC PET/CT revealed a sensitivity of 92% for adenopathy. These promising results were tempered by the relatively small number of patients and lack of histopathologic correlation (57–59) (Fig 8). The second-generation, urea-based, ^{18}F-labeled, PSMA-targeting PET agent 2-(3-(1-carboxy-5-[(6-[18F]fluoro-pyridine-3-carbonyl)-amino]-pentyl)-ureido)-pentanedioic acid (^{18}F-DCFPyl) has been reported in only one study for tumor detection in patients with PCa recurrence with superior characteristics with lower background signal and higher PSMA affinity. This agent has higher affinity and faster background clearance than does ^{18}F-DCFBC, and thus is expected to be a superior agent. A recent pilot study with nine patients with PCa recurrence showed that ^{18}F-DCFPyl revealed more lesions compared with conventional imaging methods (CT, bone scan) at which most lesions appear negative or equivocal. In this study, 139 sites of PET-positive ^{18}F-DCFPyl uptake (138 definite, one equivocal) for metastatic disease were revealed in the eight patients by using available comparison conventional imaging methods. By contrast, only 45 lesions were identified by using conventional imaging methods (30 definite, 15 equivocal). When lesions were negative or equivocal at conventional imaging, it was estimated that a large portion of these lesions or 0.72 (95% CI: 0.55, 0.84) would be positive at ^{18}F-DCFPyl PET. Conversely, of those lesions negative or equivocal at ^{18}F-DCFPyl PET, it was estimated that only a small proportion or 0.03 (95% CI: 0.01, 0.07) would be positive at conventional imaging. This study shows a promising preliminary experience for use of second-generation, ^{18}F-labeled, PSMA-targeted PET radiotracer (59,60).

A related group of PET tracers more commonly used in Europe are PSMA-targeted tracers bearing a chelate that enables labeling with ^{68}Ga. ^{68}Ga is a PET emitting isotope with a half-life of 68 minutes that is produced in an on-site generator. In a retrospective analysis with ^{68}Ga and N,N'-bis-[2-hydroxy-5-(carboxyethyl)benzyl]ethylenediamine-N,N'-diacetic acid) (HBED-CC), 42 histopathologically verified patients demonstrated a lesion-based sensitivity, specificity, negative predictive value, and positive predictive value of 76.6%, 100%, 91.4%, and 100%, respectively. A patient-based analysis revealed a sensitivity of 88.1% (61). These results demonstrate higher sensitivity and specificity than do the agents discussed previously. Less encouraging results were found in another study of 30 patients who underwent ^{68}Ga-PSMA PET/CT and radical prostatectomy. Overall sensitivity, specificity, positive predictive value, and negative predictive value of ^{68}Ga-PSMA PET/CT for detection of LN metastases were 33.3%, 100%, 100%, and 69.2%, respectively. The authors commented that similar to other staging modalities, ^{68}Ga-PSMA PET/CT is also limited in detecting tiny metastatic foci within LNs prior to radical prostatectomy when using histologic findings as the reference standard because micrometastatic tumor foci are likely to be missed (62,63). In another study of ^{68}Ga-PSMA PET/CT, 35 patients with PCa validated with ePLND (mixing staging and restaging patients) demonstrated a per-node sensitivity of 94%, specificity of 99%, positive predictive value of 89%, and negative predictive value of 99.5%. These impressive results, however, need to be tempered by the mix of patients with high-risk recurrence in the study population (64). In a recent study with 48 patients who underwent salvage lymphadenectomy following ^{68}Ga-PSMA PET, the sensitivity and specificity were reported as 77.9 and 97.3%, respectively (65) (Fig 9). This agent has mostly been used for local recurrence indication and more studies are needed for nodal staging indication,

Figure 9

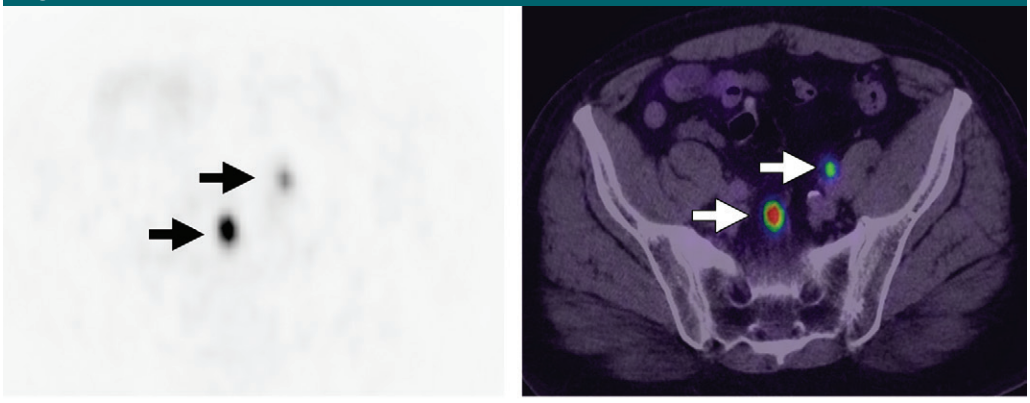

a. b.

Figure 9: Images in a 67-year-old man with PCa diagnosis. **(a)** Axial ^{68}Ga-PSMA PET and **(b)** PET/CT images show specific uptake within pelvic LNs consistent with metastatic involvement (arrows). (Image courtesy of Dr Frederik Giesel, University of Heidelberg, Heidelberg, Germany.)

in which there is currently lack of large-scale, prospective multicenter trials.

There are several reasons to consider using ^{18}F over ^{68}Ga to label the PSMA-targeting ligand. With its longer half-life and absence of chelate, this agent could be more easily commercialized and shipped to sites for use, increasing its practicality. The first preliminary comparison study included 14 patients who underwent both ^{18}F-DCFPyl and ^{68}Ga-PSMA PET imaging. ^{18}F-DCFPyl PET revealed all lesions depicted by using ^{68}Ga-PSMA PET and in three patients, ^{18}F-DCFPyl identified additional lesions, one of which was a pelvic LN. However, none of the additionally detected lesions were validated histologically (66). Currently, ^{68}Ga requires purchase of an on-site generator, which will only make sense in a high-volume setting. Additionally, there are emerging alternative radiolabeled PSMA ligands—such as PSMA-617, PSMA I&T, and MIP-1095—with imaging and therapeutic capabilities (67). PSMA-targeted PET agents have limitations such as excretion via the urinary system (obscuring pelvic uptake) and excessive blood pool activity that makes detection of metastases challenging in the vicinity of anastomoses and parailiac nodal chains, respectively; these PSMA-targeting tracers are highly specific, but the current experience is still relatively limited.

Bombesin-targeted PET Agents

Bombesin targets gastrin-releasing peptide receptor, which is overexpressed in PCa. ^{68}Ga 1,4,7,10-tetraazacyclododecane-1,4,7,10-tetraacetic acid (DOTA)-bombesin is a synthetic bombesin receptor antagonist that has been used in several small trials of PCa. It demonstrates high accumulation in the pancreas but is cleared via the kidney. The agent was recently described in humans in a small 14-patient study (68). In this study, the agent demonstrated a sensitivity of 70% for metastatic nodes by using histologic findings as the reference standard. In a recent study comparing the biodistribution of ^{68}Ga DOTA-bombesin and ^{68}Ga PSMA, the two agents behaved similarly, although the former had minimal hepatobiliary clearance whereas the latter had both renal and hepatobiliary clearance. This could mask lesions in the abdomen and pelvis (69). Although only limited clinical data are available, ^{68}Ga DOTA-bombesin appears to be competitive with other PET methods for the detection of nodal metastases.

Caveats Regarding Comparisons of PET Imaging Agents

There are several problems in using the literature to compare different PET agents. For the detection of metastatic LNs, the current literature is limited in the number of patients studied and no standards exist regarding uniformity of patient population and validation with an accepted reference standard. Another limitation is that the majority of articles tend to report patient-based results rather than lesion-based results, with the latter being more important when comparing agents. It is important to standardize the inclusion criteria and to specifically exclude patients with enlarged nodes. Validation with ePLND needs to be standardized as well. To date, limited data are available on the reproducibility of PET agents among different observers; this should be included in future studies because many studies use only a single expert observer, which may create a positive bias. The value of quantitative standardized uptake value determinations is also inadequately studied. The need to produce standardized studies with uniform inclusion and exclusion criteria and analytic methods is evident from a review of the literature.

Conclusion

Accurate LN staging of PCa is important for selecting the most appropriate treatment of PCa. Currently, such staging is done with ePLND, with its attendant adverse effects; however,

many patients do not undergo this procedure and are not properly staged. Thus, a need exists for a good imaging method for nodal staging. Current anatomic imaging based on CT and MR imaging has unacceptable limitations, as does FDG PET. Functional imaging techniques show promising results for nodal staging and depicting metastases even in normal-sized nodes. PET agents offer the possibility of increased sensitivity and specificity. Among all the methods discussed in this article and summarized in the Table, several general comments can be made. First, there is wide variation in the performance of each method, depending on the study cited and its study population and methods of validation. However, accepting the upper limits of performance, all methods described (with the possible exception of ^{11}C-acetate) have very high specificity and negative predictive values. This property is very important because false-positive results would falsely upstage the disease, potentially removing curative options for patients. However, for these agents to have high impact in the clinical setting, they must also have high sensitivity. If a study has a reputation for high false-negative results, then it would not eliminate the need for ePLND, which defeats the purpose of the staging tool (namely, reducing the number of ePLNDs). Here, the news is not so compelling because these agents and methods average sensitivities of about 70%–80% and positive predictive values of about 50% with wide variation. Sensitivity is highly dependent on prior probability based on the risk of LN involvement in the study population, and thus may be difficult to compare across studies. Achieving higher rates of sensitivity and positive predictive value will be crucial to making these tests useful for preoperative staging and allowing clinicians to rely on imaging instead of surgery. Restricting patient entry into studies to high-risk cancers may be important in using functional and molecular imaging for staging. One ray of hope comes from the PSMA-targeting PET agents that appear to have both improved sensitivity for nodal metastases and high specificity, although there is wide variation in performance. Significant practical limitations also need to be considered, including the lack of availability of suitable commercial USPIOs, the short half-life of compounds labeled with ^{11}C, the lack of ^{68}Ga generators, and the lack of commercial sources for compounds labeled with ^{18}F. These latter points, however, are secondary to the limitation that none of these methods has been proven accurate enough to replace a meticulous ePLND. However, as an intermediate step, such imaging methods may be important in defining those nodes that are positive, thus enabling the surgeon to plan the extent of the dissection more accurately. The possibility of combining PET with DW whole-body MR imaging and/or USPIO-enhanced MR imaging merits consideration now that PET/MR imagers are becoming more widespread, but it is unclear whether the two modalities would be duplicative or additive. However, before these methods can be integrated into routine clinical practice, there must be studies comparing these methods in a uniform and head-to-head manner by using ePLND for validation.

Disclosures of Conflicts of Interest: H.C.T. Activities related to the present article: disclosed no relevant relationships. Activities not related to the present article: reported a grant from Nano-Tera. Other relationships: serves as member of advisory board for Guerbet. **S.B.** Activities related to the present article: reported a grant from Nano-Tera. Activities not related to the present article: disclosed no relevant relationships. Other relationships: disclosed no relevant relationships. **J.M.F.** Activities related to the present article: disclosed no relevant relationships. Activities not related to the present article: reported consultancies for Guerbet, Mallinckrodt, and Akroswiss. Other relationships: disclosed no relevant relationships. **B.T.** disclosed no relevant relationships. **P.L.C.** disclosed no relevant relationships.

References

1. Cheng L, Montironi R, Bostwick DG, Lopez-Beltran A, Berney DM. Staging of prostate cancer. Histopathology 2012;60(1):87–117.
2. Bader P, Burkhard FC, Markwalder R, Studer UE. Disease progression and survival of patients with positive lymph nodes after radical prostatectomy. Is there a chance of cure? J Urol 2003;169(3):849–854.
3. Heidenreich A, Ohlmann CH, Polyakov S. Anatomical extent of pelvic lymphadenectomy in patients undergoing radical prostatectomy. Eur Urol 2007;52(1):29–37.
4. Thoeny HC, Froehlich JM, Triantafyllou M, et al. Metastases in normal-sized pelvic lymph nodes: detection with diffusion-weighted MR imaging. Radiology 2014;273(1):125–135.
5. Makarov DV, Trock BJ, Humphreys EB, et al. Updated nomogram to predict pathologic stage of prostate cancer given prostate-specific antigen level, clinical stage, and biopsy Gleason score (Partin tables) based on cases from 2000 to 2005. Urology 2007;69(6):1095–1101.
6. Bivalacqua TJ, Pierorazio PM, Gorin MA, Allaf ME, Carter HB, Walsh PC. Anatomic extent of pelvic lymph node dissection: impact on long-term cancer-specific outcomes in men with positive lymph nodes at time of radical prostatectomy. Urology 2013;82(3):653–658.
7. Yuh BE, Ruel NH, Mejia R, Novara G, Wilson TG. Standardized comparison of robot-assisted limited and extended pelvic lymphadenectomy for prostate cancer. BJU Int 2013;112(1):81–88.
8. Staník M, Čapák I, Macík D, et al. Sentinel lymph node dissection combined with meticulous histology increases the detection rate of nodal metastases in prostate cancer. Int Urol Nephrol 2014;46(8):1543–1549.
9. Schiavina R, Capizzi E, Borghesi M, et al. Nodal occult metastases in intermediate- and high-risk prostate cancer patients detected using serial section, immunohistochemistry, and real-time reverse transcriptase polymerase chain reaction: prospective evaluation with matched-pair analysis. Clin Genitourin Cancer 2015;13(2):e55–e64.
10. Ledezma RA, Negron E, Razmaria AA, et al. Robotic-assisted pelvic lymph node dissection for prostate cancer: frequency of nodal metastases and oncological outcomes. World J Urol 2015;33(11):1689–1694.
11. Withdrawal assessment report for Sinerem. European Medicines Agency. http://www.ema.europa.eu/docs/en_GB/document_library/Application_withdrawal_assessment_report/2010/01/WC500067463.pdf. Published February 21, 2008. Accessed January 19, 2017.
12. Harisinghani MG, Saksena MA, Hahn PF, et al. Ferumoxtran-10-enhanced MR lymphangiography: does contrast-enhanced imaging alone suffice for accurate lymph node

characterization? AJR Am J Roentgenol 2006;186(1):144–148.

13. Froehlich JM, Triantafyllou M, Fleischmann A, Vermathen P, Thalmann GN, Thoeny HC. Does quantification of USPIO uptake-related signal loss allow differentiation of benign and malignant normal-sized pelvic lymph nodes? Contrast Media Mol Imaging 2012;7(3):346–355.
14. Harisinghani MG, Barentsz J, Hahn PF, et al. Noninvasive detection of clinically occult lymph-node metastases in prostate cancer. N Engl J Med 2003;348(25):2491–2499.
15. Heesakkers RA, Jager GJ, Hövels AM, et al. Prostate cancer: detection of lymph node metastases outside the routine surgical area with ferumoxtran-10-enhanced MR imaging. Radiology 2009;251(2):408–414.
16. Fortuin AS, Deserno WM, Meijer HJ, et al. Value of PET/CT and MR lymphography in treatment of prostate cancer patients with lymph node metastases. Int J Radiat Oncol Biol Phys 2012;84(3):712–718.
17. Heesakkers RA, Hövels AM, Jager GJ, et al. MRI with a lymph-node-specific contrast agent as an alternative to CT scan and lymph-node dissection in patients with prostate cancer: a prospective multicohort study. Lancet Oncol 2008;9(9):850–856.
18. Deserno WM, Harisinghani MG, Taupitz M, et al. Urinary bladder cancer: preoperative nodal staging with ferumoxtran-10-enhanced MR imaging. Radiology 2004;233(2):449–456.
19. Briganti A, Rigatti P, Montorsi F. The importance of the extent of pelvic-lymph-node dissection in the diagnosis of lymph-node metastases in prostate cancer. Lancet Oncol 2008;9(10):915–917; author reply 917–918.
20. Triantafyllou M, Studer UE, Birkhäuser FD, et al. Ultrasmall superparamagnetic particles of iron oxide allow for the detection of metastases in normal sized pelvic lymph nodes of patients with bladder and/or prostate cancer. Eur J Cancer 2013;49(3):616–624.
21. Bernd H, De Kerviler E, Gaillard S, Bonnemain B. Safety and tolerability of ultrasmall superparamagnetic iron oxide contrast agent: comprehensive analysis of a clinical development program. Invest Radiol 2009;44(6):336–342.
22. Provenzano R, Schiller B, Rao M, Coyne D, Brenner L, Pereira BJ. Ferumoxytol as an intravenous iron replacement therapy in hemodialysis patients. Clin J Am Soc Nephrol 2009;4(2):386–393.
23. Landry R, Jacobs PM, Davis R, Shenouda M, Bolton WK. Pharmacokinetic study of ferumoxytol: a new iron replacement therapy in normal subjects and hemodialysis patients. Am J Nephrol 2005;25(4):400–410.
24. Spinowitz BS, Schwenk MH, Jacobs PM, et al. The safety and efficacy of ferumoxytol therapy in anemic chronic kidney disease patients. Kidney Int 2005;68(4):1801–1807.
25. Harisinghani M, Ross RW, Guimaraes AR, Weissleder R. Utility of a new bolus-injectable nanoparticle for clinical cancer staging. Neoplasia 2007;9(12):1160–1165.
26. Turkbey B, Agarwal HK, Shih J, et al. A phase I dosing study of ferumoxytol for MR lymphography at 3 T in patients with prostate cancer. AJR Am J Roentgenol 2015;205(1):64–69.
27. Feraheme (ferumoxytol): Drug safety communication—warnings strengthened and prescribing instructions changed. U.S. Food and Drug Administration. http://www.fda.gov/Safety/MedWatch/SafetyInformation/SafetyAlertsforHumanMedicalProducts/ucm440479.htm. Published March 31, 2015. Accessed June 29, 2016.
28. Kobus T, van der Laak JA, Maas MC, et al. Contribution of histopathologic tissue composition to quantitative MR spectroscopy and diffusion-weighted imaging of the prostate. Radiology 2016;278(3):801–811.
29. Chatterjee A, Watson G, Myint E, Sved P, McEntee M, Bourne R. Changes in epithelium, stroma, and lumen space correlate more strongly with Gleason pattern and are stronger predictors of prostate ADC changes than cellularity metrics. Radiology 2015;277(3):751–762.
30. Kim JK, Kim KA, Park BW, Kim N, Cho KS. Feasibility of diffusion-weighted imaging in the differentiation of metastatic from non-metastatic lymph nodes: early experience. J Magn Reson Imaging 2008;28(3):714–719.
31. Eiber M, Beer AJ, Holzapfel K, et al. Preliminary results for characterization of pelvic lymph nodes in patients with prostate cancer by diffusion-weighted MR-imaging. Invest Radiol 2010;45(1):15–23.
32. Papalia R, Simone G, Grasso R, et al. Diffusion-weighted magnetic resonance imaging in patients selected for radical cystectomy: detection rate of pelvic lymph node metastases. BJU Int 2012;109(7):1031–1036.
33. Park SY, Oh YT, Jung DC, Cho NH, Choi YD, Rha KH. Prediction of micrometastasis (< 1 cm) to pelvic lymph nodes in prostate cancer: role of preoperative MRI. AJR Am J Roentgenol 2015;205(3):W328–W334.
34. Roy C, Bierry G, Matau A, Bazille G, Pasquali R. Value of diffusion-weighted imaging to detect small malignant pelvic lymph nodes at 3 T. Eur Radiol 2010;20(8):1803–1811.
35. Mir N, Sohaib SA, Collins D, Koh DM. Fusion of high b-value diffusion-weighted and T2-weighted MR images improves identification of lymph nodes in the pelvis. J Med Imaging Radiat Oncol 2010;54(4):358–364.
36. Birkhäuser FD, Studer UE, Froehlich JM, et al. Combined ultrasmall superparamagnetic particles of iron oxide-enhanced and diffusion-weighted magnetic resonance imaging facilitates detection of metastases in normal-sized pelvic lymph nodes of patients with bladder and prostate cancer. Eur Urol 2013;64(6):953–960.
37. Thoeny HC, Triantafyllou M, Birkhaeuser FD, et al. Combined ultrasmall superparamagnetic particles of iron oxide-enhanced and diffusion-weighted magnetic resonance imaging reliably detect pelvic lymph node metastases in normal-sized nodes of bladder and prostate cancer patients. Eur Urol 2009;55(4):761–769.
38. Beauregard JM, Blouin AC, Fradet V, et al. FDG-PET/CT for pre-operative staging and prognostic stratification of patients with high-grade prostate cancer at biopsy. Cancer Imaging 2015;15:2.
39. Vag T, Heck MM, Beer AJ, et al. Preoperative lymph node staging in patients with primary prostate cancer: comparison and correlation of quantitative imaging parameters in diffusion-weighted imaging and 11C-choline PET/CT. Eur Radiol 2014;24(8):1821–1826. [Published correction appears in Eur Radiol 2014;24(8):1827.]
40. Fanti S, Minozzi S, Castellucci P, et al. PET/CT with (11)C-choline for evaluation of prostate cancer patients with biochemical recurrence: meta-analysis and critical review of available data. Eur J Nucl Med Mol Imaging 2016;43(1):55–69.
41. Kotzerke J, Prang J, Neumaier B, et al. Experience with carbon-11 choline positron emission tomography in prostate carcinoma. Eur J Nucl Med 2000;27(9):1415–1419.
42. Poulsen MH, Bouchelouche K, Høilund-Carlsen PF, et al. [18F]fluoromethylcholine (FCH) positron emission tomography/computed tomography (PET/CT) for lymph node staging of prostate cancer: a prospective study of 210 patients. BJU Int 2012;110(11):1666–1671.
43. Evangelista L, Guttilla A, Zattoni F, Muzzio PC, Zattoni F. Utility of choline positron emission tomography/computed tomography for lymph node involvement identification in intermediate- to high-risk prostate cancer: a systematic literature review and meta-analysis. Eur Urol 2013;63(6):1040–1048.
44. Grassi I, Nanni C, Allegri V, et al. The clinical use of PET with (11)C-acetate. Am J Nucl Med Mol Imaging 2012;2(1):33–47.
45. Schumacher MC, Radecka E, Hellström M, Jacobsson H, Sundin A. [11C]Acetate positron emission tomography-computed tomog-

raphy imaging of prostate cancer lymph-node metastases correlated with histopathological findings after extended lymphadenectomy. Scand J Urol 2015;49(1):35–42.

46. Haseebuddin M, Dehdashti F, Siegel BA, et al. 11C-acetate PET/CT before radical prostatectomy: nodal staging and treatment failure prediction. J Nucl Med 2013;54(5):699–706.

47. Mohsen B, Giorgio T, Rasoul ZS, et al. Application of C-11-acetate positron-emission tomography (PET) imaging in prostate cancer: systematic review and meta-analysis of the literature. BJU Int 2013;112(8):1062–1072.

48. Oka S, Hattori R, Kurosaki F, et al. A preliminary study of anti-1-amino-3-18F-fluorocyclobutyl-1-carboxylic acid for the detection of prostate cancer. J Nucl Med 2007;48(1):46–55.

49. Schuster DM, Votaw JR, Nieh PT, et al. Initial experience with the radiotracer anti-1-amino-3-18F-fluorocyclobutane-1-carboxylic acid with PET/CT in prostate carcinoma. J Nucl Med 2007;48(1):56–63.

50. Nanni C, Schiavina R, Brunocilla E, et al. 18F-FACBC compared with 11C-choline PET/CT in patients with biochemical relapse after radical prostatectomy: a prospective study in 28 patients. Clin Genitourin Cancer 2014;12(2):106–110.

51. Wright GL Jr, Haley C, Beckett ML, Schellhammer PF. Expression of prostate-specific membrane antigen in normal, benign, and malignant prostate tissues. Urol Oncol 1995;1(1):18–28.

52. Schettino CJ, Kramer EL, Noz ME, Taneja S, Padmanabhan P, Lepor H. Impact of fusion of indium-111 capromab pendetide volume data sets with those from MRI or CT in patients with recurrent prostate cancer. AJR Am J Roentgenol 2004;183(2):519–524.

53. Han D, Wu J, Han Y, et al. A novel anti-PSMA human scFv has the potential to be used as a diagnostic tool in prostate cancer. Oncotarget 2016;7(37):59471–59481.

54. Mazzocco C, Fracasso G, Germain-Genevois C, et al. In vivo imaging of prostate cancer using an anti-PSMA scFv fragment as a probe. Sci Rep 2016;6:23314.

55. Mease RC, Foss CA, Pomper MG. PET imaging in prostate cancer: focus on prostate-specific membrane antigen. Curr Top Med Chem 2013;13(8):951–962.

56. 18F-DCFBC PET/CT in prostate cancer. National Cancer Institute. https://clinicaltrials.gov/show/NCT02190279. Published July 12, 2014. Accessed January 19, 2017.

57. Rowe SP, Macura KJ, Ciarallo A, et al. Comparison of prostate-specific membrane antigen-based 18F-DCFBC PET/CT to conventional imaging modalities for detection of hormone-naïve and castration-resistant metastatic prostate cancer. J Nucl Med 2016;57(1):46–53.

58. Cho SY, Gage KL, Mease RC, et al. Biodistribution, tumor detection, and radiation dosimetry of 18F-DCFBC, a low-molecular-weight inhibitor of prostate-specific membrane antigen, in patients with metastatic prostate cancer. J Nucl Med 2012;53(12):1883–1891.

59. Rowe SP, Macura KJ, Mena E, et al. PSMA-based [(18)F]DCFPyL PET/CT is superior to conventional imaging for lesion detection in patients with metastatic prostate cancer. Mol Imaging Biol 2016;18(3):411–419.

60. Szabo Z, Mena E, Rowe SP, et al. Initial evaluation of [(18)F]DCFPyL for prostate-specific membrane antigen (PSMA)-targeted PET imaging of prostate cancer. Mol Imaging Biol 2015;17(4):565–574.

61. Afshar-Oromieh A, Avtzi E, Giesel FL, et al. The diagnostic value of PET/CT imaging with the (68)Ga-labelled PSMA ligand HBED-CC in the diagnosis of recurrent prostate cancer. Eur J Nucl Med Mol Imaging 2015;42(2):197–209.

62. Freitag MT, Radtke JP, Hadaschik BA, et al. Comparison of hybrid (68)Ga-PSMA PET/MRI and (68)Ga-PSMA PET/CT in the evaluation of lymph node and bone metastases of prostate cancer. Eur J Nucl Med Mol Imaging 2016;43(1):70–83.

63. Budäus L, Leyh-Bannurah SR, Salomon G, et al. Initial experience of (68)Ga-PSMA PET/CT imaging in high-risk prostate cancer patients prior to radical prostatectomy. Eur Urol 2016;69(3):393–396.

64. Hijazi S, Meller B, Leitsmann C, et al. Pelvic lymph node dissection for nodal oligometastatic prostate cancer detected by 68Ga-PSMA-positron emission tomography/computerized tomography. Prostate 2015;75(16):1934–1940.

65. Rauscher I, Maurer T, Beer AJ, et al. Value of 68Ga-PSMA HBED-CC PET for the assessment of lymph node metastases in prostate cancer patients with biochemical recurrence: comparison with histopathology after salvage lymphadenectomy. J Nucl Med 2016;57(11):1713–1719.

66. Dietlein M, Kobe C, Kuhnert G, et al. Comparison of [(18)F]DCFPyL and [(68) Ga]Ga-PSMA-HBED-CC for PSMA-PET imaging in patients with relapsed prostate cancer. Mol Imaging Biol 2015;17(4):575–584.

67. Afshar-Oromieh A, Babich JW, Kratochwil C, et al. The rise of PSMA ligands for diagnosis and therapy of prostate cancer. J Nucl Med 2016;57(Suppl 3):79S–89S.

68. Kähkönen E, Jambor I, Kemppainen J, et al. In vivo imaging of prostate cancer using [68Ga]-labeled bombesin analog BAY86-7548. Clin Cancer Res 2013;19(19):5434–5443.

69. Minamimoto R, Hancock S, Schneider B, et al. Pilot comparison of ^{68}Ga-RM2 PET and ^{68}Ga-PSMA-11 PET in patients with biochemically recurrent prostate cancer. J Nucl Med 2016;57(4):557–562.